Soil Dynamics and Earthquake Engineering 128 (2020) 105868

Contents lists available at ScienceDirect

Soil Dynamics and Earthquake Engineering

journal homepage: www.elsevier.com/locate/soildyn

Seismic evaluation of precast bridge columns with built-in elastomeric pads

Junfeng Jia[a,*], Kaidi Zhang[a], M. Saiid Saiidi[b], Yang Guo[a], Suiwen Wu[b], Kaiming Bi[c], Xiuli Du[a]

[a] Key Laboratory of Urban Security and Disaster Engineering of Ministry of Education, Beijing University of Technology, Beijing, 100124, China
[b] Department of Civil and Environmental Engineering, University of Nevada, Reno, NV, 89557, USA
[c] Centre for Infrastructure Monitoring and Protection, School of Civil and Mechanical Engineering, Curtin University, Kent Street, Bentley, WA, 6102, Australia

ARTICLE INFO

Keywords:
Precast bridge column
Accelerated bridge construction
Elastomeric pad
Pseudo-static cyclic test
Seismic evaluation
Grouted corrugated duct connection

ABSTRACT

A novel built-in elastomeric pad was incorporated into the plastic hinge zone of precast bridge columns with grouted corrugated duct connection to improve its seismic performance. Appropriate energy dissipation and minimal local concrete damage are expected in the innovative precast reinforced concrete (RC) columns. Four 1/4-scaled bridge column specimens were designed and tested under constant axial compression force and cyclic lateral loads to evaluate the feasibility and effectiveness of the proposed concept. Detailed experiment results were compared and discussed. The testing results showed that the main seismic index of precast RC bridge columns with grouted metal corrugated duct connection was similar to that of the cast-in-place bridge columns. It was also found that the precast RC column with a built-in elastomeric pad in the plastic hinge zone effectively minimized local concrete damage at the bottom of bridge columns and increased the energy dissipation capacity. The laminated elastomeric pad is recommended to be applied in the precast bridge column to maintain necessary initial stiffness and energy dissipation capacity and to avoid lateral bulge of single thick rubber. Excessive buckling and shear deformations of longitudinal rebars should be prevented by inserting a rectangular or square steel tube at the center of the elastomeric pad.

1. Introduction

Accelerated bridge construction (ABC) provides many advantages over the conventional cast-in-place construction methods such as shorter onsite construction time, less traffic impact, potentially lower lifespan costs, increased safety for workers, improved quality and durability of precast members [1–3]. It has become a trend for the next generation of bridge structures. Prefabricated bridge elements and systems are essential parts of ABC technique. Precast girders have been widely used in the conventional highway and railway bridge constructions, but prefabricated bridge substructures are used relatively less frequently. Previous projects with prefabricated bridge columns are mainly for bridges in low seismic regions. Applications of precast bridge substructures in high seismic regions are limited due to the lack of sufficient information on seismic performance of precast bridge connections [4–7].

1.1. Grouted corrugated duct connection for ABC

The reliability of the connection between bridge segments and joints is the most important factor that affects the seismic performance of precast bridge structures. To design reliable joint connections, the U.S. National Cooperative Highway Research Program (NCHRP) has conducted a series of studies on the connection forms for the column-to-cap beam or column-to-footing joints including the mechanical bar coupler connections, grouted duct connections, pocket and socket connections and rocking systems [8–11]. The grouted corrugated duct connection was recommended due to its fast construction, reliable performance, and allowing larger construction tolerances [6,12]. Some researchers have carried out to investigate grouted corrugated duct connections in precast bridge substructures. Matsumoto et al. [13] investigated the bond-slip performance between grouted metal corrugated ducts and anchored steel bars based on pull-out tests, and their tests results showed that using grouted metal corrugated ducts to anchor steel bars showed satisfactory performance and ductility. Brenes et al. [14] carried out large-scale pull-out tests to investigate parameters of grouted metal corrugated ducts that may influence the connection performance. They further proposed a formula to calculate anchorage the length of anchored steel rebars. The high-strength low-shrinking grouting material was adopted to enhance bond performance of grouted metal corrugated ducts. It was found that sufficient bonding strength between anchored bars and grouted metal corrugated ducts and integral performance of precast structures could be achieved [15,16]. Mashal and Palermo [3], Belleri et al. [17], and Popa et al. [18] compared seismic

* Corresponding author.
E-mail address: jiajunfeng@bjut.edu.cn (J. Jia).

https://doi.org/10.1016/j.soildyn.2019.105868
Received 17 May 2019; Received in revised form 9 September 2019; Accepted 18 September 2019

performance of precast columns with grouted corrugated duct connection and cast-in-place columns. They concluded that horizontal loading capacity of precast columns with the grouted corrugated duct connection was similar to that of cast-in-place columns, but larger grouting layer damage and residual displacement were found in the precast columns. Recently, the ultra-high-performance concrete (UHPC) was used as the grouting material, and but no obvious advantages were reported compared to the high-strength non-shrinking grouting material [19].

1.2. Measures to mitigate local damage in columns

Previous studies revealed that serious concrete damage may occur at the plastic hinge zone of columns [20,21]. A few researchers have investigated the feasibility of advanced materials and construction details to reduce or eliminate local damage of precast bridge substructures. As one of the innovative materials and construction details, elastomeric pad was proposed and investigated to minimize local damage and residual deformation. Elastomeric pad has been applied in civil engineering for more than 40 years as base isolators to elongate structural fundamental period and reduce seismic vibration responses. In 2002, Kwashima and Nagai incorporated elastomeric pads into the plastic hinge region of cast-in-place concrete bridge columns to eliminate concrete spalling and reduce local damage in the plastic hinge region [22]. The performance was satisfactory up to moderate levels of lateral displacements, but the elastomeric pad did not provide sufficient lateral restraint for longitudinal reinforcement under large lateral displacements. The column rebars buckled and fractured under low cyclic loading. Saiidi and his research team developed a modified version of elastomeric pads in precast post-tensioned bridge piers [23–26]. They incorporated steel shims into the elastomeric pad to prevent rebar buckling. In their design, the pad was relatively thick to allow the column for large rotation. A central steel pipe was inserted into the footing and column to resist shear force, which also served as a duct for post-tensioned strands, which provided re-centering capacity to minimize residual displacements. It was found that the precast post-tensioned segmental bridge piers with built-in elastomeric pads showed high energy dissipation, minimal damage in the plastic hinge zone, appropriate lateral load capacity, and minimal residual displacement. The conclusion was then made that the proposed models with advanced materials and details are suitable for accelerated bridge construction in high seismic zones. Kheyroddin and Dabiri [27] used elastomeric materials in a RC pier to diminish or even eliminate corrosion of reinforcement bars, large base shear and tensile defect of concrete. Elastomeric material was used in plastic hinge zone of RC piers in different heights and thicknesses. Results showed that using elastomeric material in a RC pier reduced ductility but would decrease base shear by 10.61%, with the advantage of eliminating concrete tensile defect in tension side of pier section and reinforcement bars corrosion due to concrete cover ruin in corrosive environment. Above-mentioned limited researches on application of built-in elastomeric pads were mainly in cast-in-situ bridge piers or precast post-tensioned segmental bridge piers, primarily proving the feasibility and efficiency of this advanced material and innovative detail.

1.3. Purpose and contents of this study

Built on the aforementioned concept and design detail of precast bridge columns and built-in elastomeric pad, an innovative design concept and details of incorporating a built-in elastomeric pad into the precast bridge column with the grouted corrugated metal duct connection was proposed to minimize local concrete damage in the plastic hinge zones and to maintain appropriate energy dissipation capacity. Four 1/4-scaled RC bridge column specimens with different design concepts and details were designed and constructed, including a cast-in-place RC column (CIP), a precast RC column with grouted metal corrugated duct connection (GCP), a GCP column with a built-in laminated elastomeric pad (GCP-M), and a GCP column with a single-layer elastomeric pad (GCP-S). These columns were tested under constant axial force and cyclic lateral loads. The seismic performance including lateral strength, displacement ductility, energy dissipation capacity, was investigated and discussed to evaluate the feasibility and efficiency of precast bridge columns with the grouted corrugated duct connection and built-in elastomeric pad at the bottom of the precast RC bridge column.

2. Experimental design

2.1. Design and construction of specimens

A typical three-span continuous PC box-girder bridge constructed by cast-in-place method in Beijing, China, was selected as the prototype bridge in this study. The bridge with length of 3 × 30 m was designed based on the *Specifications for Design of Highway Reinforced Concrete and Prestressed Concrete Bridges and Culverts* (JTG 3362-2018) [28] and the *Guidelines for Seismic Design of Highway Bridges*(JTG/T B02-01-2008) [29]. The pier is a two-column bent with a height of 6.4 m and a diameter of 1.6 m. The bridge is located in the urban area with a design peak ground acceleration (PGA) of 0.2 g. Four 1/4-scaled bridge column specimens were designed according to the prototype columns. The aspect ratio, reinforcement ratio and axial load index of scaled columns were consistent with the prototype. The cast-in-place RC bridge column (CIP) was a benchmark specimen. The GCP specimen was to verify seismic performance of typical precast bridge columns using grouted corrugated duct connection. The GCP-M and GCP-S specimens were designed to explore potential advanced seismic resistance of precast bridge columns, incorporating laminated and single-layer elastomeric pad, respectively. The main design parameters of these four specimens are shown in Table 1. The diameter of these RC bridge column specimens was 400 mm and the calculated height, which was defined as the height from the bottom of bridge columns to lateral loading center, was 1600 mm. The aspect ratio defined as the height of the RC bridge column divided by the diameter of the column or elastomeric pad was designed to be 4.0. Therefore, the failure mode of these

Table 1
Design parameters of different specimens.

Specimen	Longitudinal rebar		Spiral stirrups		Precast Y/N	ALI	Column-to-footing Joint
	Size	Area ratio	Size	VTR			
CIP	12ϕ16 HRB400	1.92%	ϕ8@50mm HRB335	1.20%	NO	0.133	Casting-in-situ
GCP	12ϕ16 HRB400	1.92%	ϕ8@50mm HRB335	1.20%	YES	0.133	High-Strength grout joints
GCP-M	12ϕ16 HRB400	1.92%	ϕ8@50mm HRB335	1.20%	YES	0.133	Laminated elastomeric bearing
GCP-S	12ϕ16 HRB400	1.92%	ϕ8@50mm HRB335	1.20%	YES	0.133	Single-layer elastomeric bearing

Note: HRB is the abbreviation of Hot-rolled Ribbed Bar in China. HRB335 and HRB 400 were two types of main commonly used steel rebars in engineering structures. VTR represents volumetric transverse ratio.

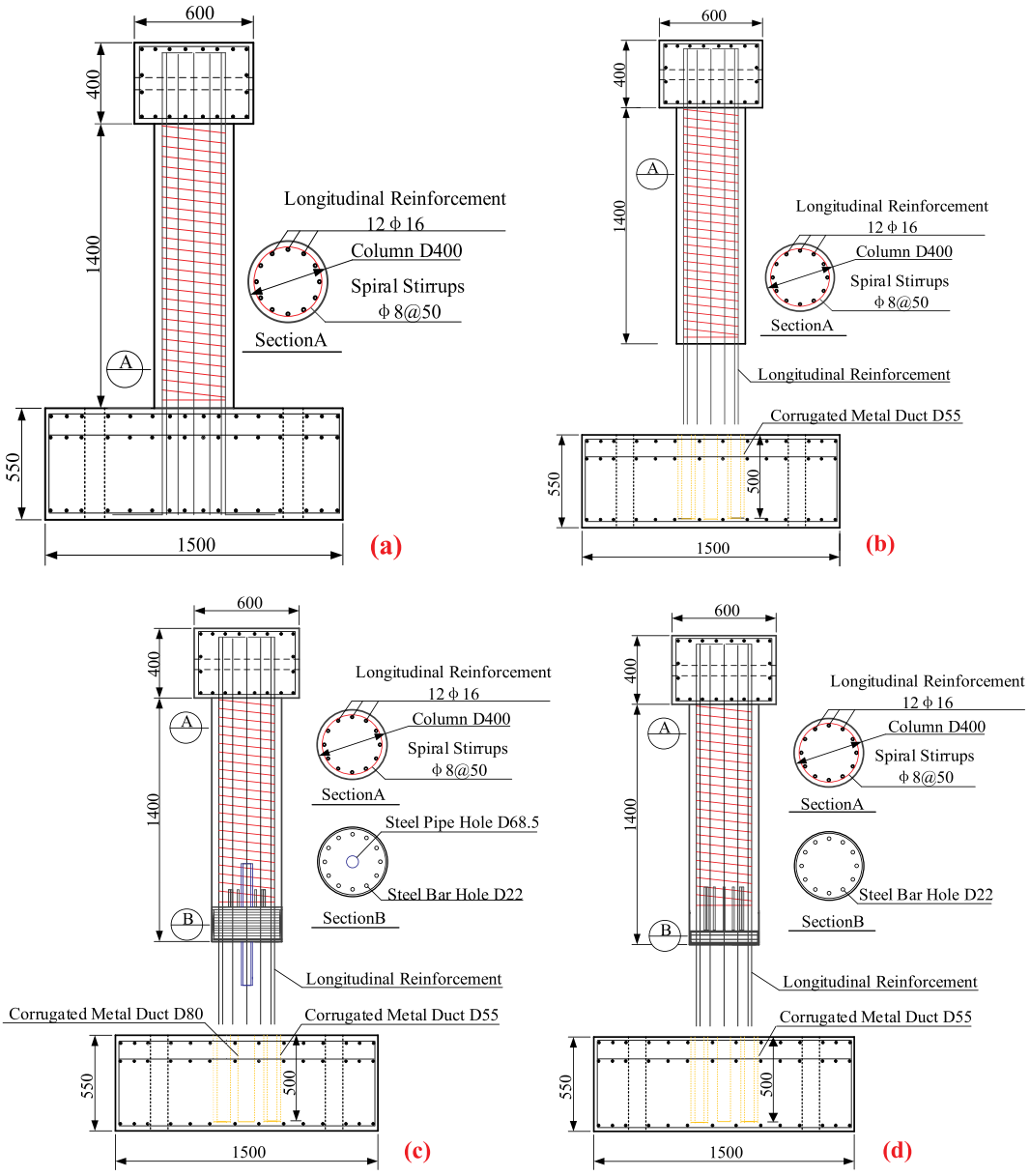

Fig. 1. Geometry and design details of specimens (unit: mm): (a) CIP; (b) GCP; (c) GCP-M; (d) GCP-S.

columns would be dominated by flexure loads. Twelve longitudinal reinforcement steel bars with a diameter of 16 mm were uniformly installed around the cross section of the bridge column. The diameter of the transverse rebar was 8 mm and the spacing of reinforcing stirrups was 50 mm. The thickness of cover concrete was 25 mm. The axial load index (ALI), defined as the ratio of applied axial load to compressive strength of the column, was designed as 0.133 for these four specimens.

Fig. 1(a)–1(d) show the structural details of CIP, GCP, GCP-M, and GCP-S models respectively. As seen in Fig. 1, a loading block with dimensions of 400 mm × 600 mm × 600mm was designed on the top of each model in order to connect with the horizontal actuator. As seen in Fig. 1 (a), for CIP specimen (traditional RC bridge column), reinforcement bars in bridge columns and footings formed an intact reinforcement cage, and the concrete was casted at one time. It is seen in Fig. 1(b) that the construction detail of the GCP specimen was substantially different with that of the CIP specimen. The longitudinal reinforcement bars extended from the bottom of the bridge column for connecting the footing. Corresponding to the longitudinal reinforcement, corrugated metal ducts with a certain anchorage length were pre-embedded into the footing. As seen in Fig. 1(c), the GCP-M specimen, which was designed based on the GCP specimen, incorporated a laminated elastomeric pad in the plastic hinge zone of the bridge column. According to clause 7.4.3 in the *Guidelines for Seismic Design of Highway Bridges* (JTG/T B02-01-2008) [30], the equivalent plastic hinge length of the column is whichever is less in Formulas (1) and (2):

$$L_p = 0.08H + 0.022f_y d_s \geq 0.044f_y d_s \tag{1}$$

$$L_p = \frac{2}{3}b \tag{2}$$

In which, L_p is the equivalent plastic hinge length (unit: cm), H is height of the cantilever column (unit: cm), f_y is diameter and standard value of yield strength of longitudinal steel rebars (unit: MPa), d_s is diameter of longitudinal steel rebars, b is diameter of the column. Therefore, the equivalent plastic hinge length was 267 mm. Since the height of laminated elastomeric pad would impose more flexible moment-resistance of whole RC column, a slightly smaller height of 200 mm was selected as the height of the laminated elastomeric pad. The laminated elastomeric pad was composed of 34 rubber layers and

GCP-M; (d) GCP-S.

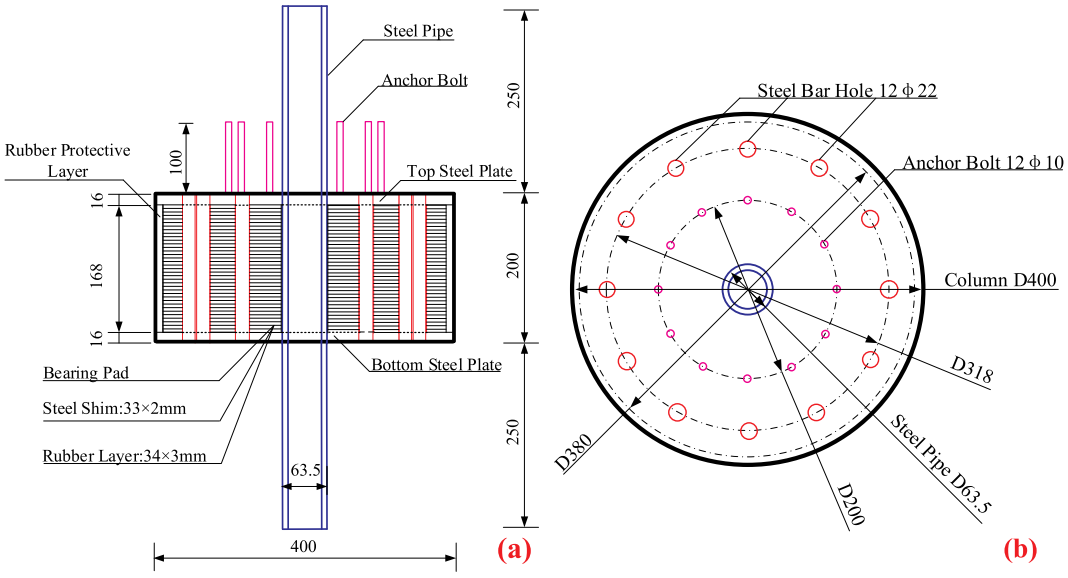

Fig. 2. Laminated rubber pad (unit: mm): (a) elevation view; (b) plan view.

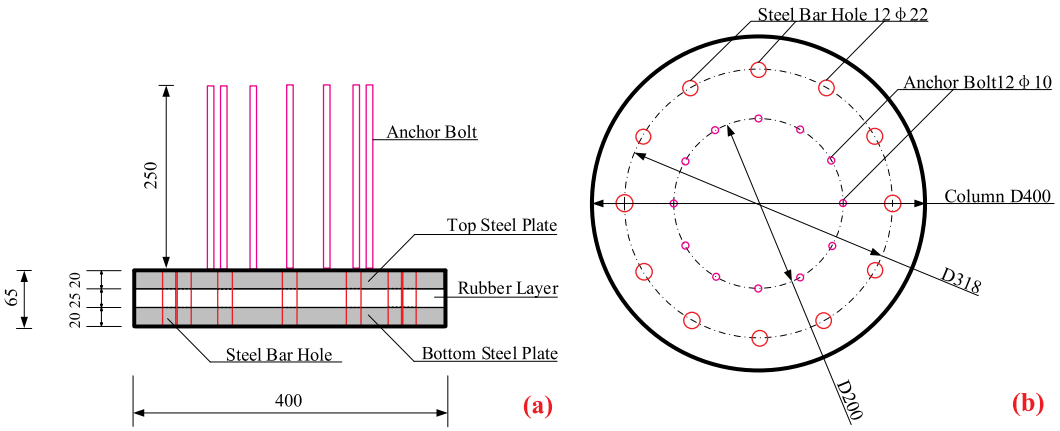

Fig. 3. Single rubber pad in GCP-S (unit: mm): (a) elevation view, (b) plan view.

33 steel shims, and two connection plates with the thickness of 16 mm as shown in Fig. 2. The thickness was 3 mm and 2 mm for each layer of rubber and steel shim, respectively. An extra strong steel pipe with outer diameter of 63.5mm and thickness of 8 mm was inserted into the elastomeric pad and extended out 250 mm to resist shear force in the bottom of the GCP-M specimen. Twelve anchor bolts with length of 100 mm and diameter of 16 mm were screwed into the upper connection plate to enhance the connection between RC column and the elastomeric pad. Twelve perforated holes with diameter of 22 mm were drilled uniformly along circumference to allow the corresponding longitudinal reinforcement of RC bridge column passing through the laminated elastomeric pad. As seen in Fig. 1(d), the GCP-S specimen incorporated a single-layer elastomeric pad into the bottom of the GCP specimen. The total height of the single-layer elastomeric pad was 65 mm, as shown in Fig. 3. The built-in single-layer elastomeric pad was composed of a rubber shim with a thickness of 25 mm and two connection steel plates with the thickness of 20 mm. The length and diameter of anchored 12 bolts were 250 mm and 16 mm to connect the elastomeric pad with RC bridge column. As seen from Figs. 2(a) and 3(a), there was no anchor bolt to connect the pad to the foundation. This is due to the difficulty in constructing this detail during installation of the bridge columns on site. In addition, the strong foundation is usually stronger than the column and always remains elastic during earthquake load. Lack of additional anchored bolts between bottom of elastomeric pad and foundation will not influence the behavior of this connection. There was no central steel pipe for shear resistance in the single-layer elastomeric pad. This is mainly because the single-layer elastomeric pad in the GCP-S specimen had notably smaller height compared with the laminated pad in the GCP-M specimen. Accordingly, the shear resistance provided by the shorter pads and the shorter longitudinal rebars within the pads can provide adequate and larger shear resistance than those in the GCP-M specimen. Therefore, the shear deformation of the single-layer elastomeric pad was supposed to be small and have a slight effect on the lateral resistance capacity of the GCP-S specimen.

Fig. 4 shows the schematic diagram and photos of construction process of the GCP-M specimen. The construction procedure consisted of three steps. In the first step, the reinforcement cages of the footing and column were prepared, and the corrugated metal ducts were fastened at the designed position. It is noted that the footing and RC column were prefabricated separately. A circular hole corresponding to the steel pipe in the center of the laminated elastomeric pad was reserved in the column and the footing, respectively. In the second step, the extended longitudinal reinforcement from the column was then

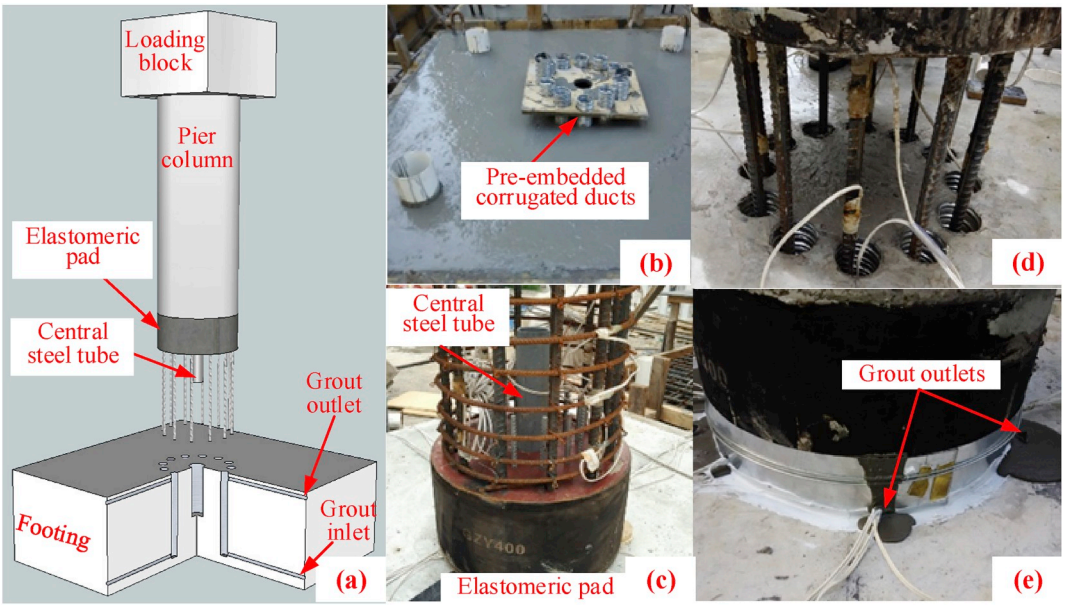

Fig. 4. Construction procedure of GCP-M specimen, (1) schematic diagram, (b) precast footing with embedded corrugated metal ducts, (c) longitudinal rebars inserting to corrugated metal ducts, (d) reinforcement cage of the bridge column with a built-in elastomeric pad, (e) grouting joint gap.

inserted into embedded corrugated metal ducts in footing when the cured-concrete strength reached design value. Several small cushion blocks were placed between the footing and the bottom surface of the column to form a small gap and to adjust the perpendicularity of the bridge column. In the last step, a circular iron sheet with two or more outlet holes was fixed outside the joint gap between the precast column and the precast footing. Low-shrinkage high performance grouts were pumped into corrugated metal ducts and the joint gap through inlet grouting pipes. The construction detail and process of the GCP and GCP-S specimens were similar to the GCP-M specimen. The main differences were that there was no built-in elastomeric pad at the bottom of the bridge column in the GCP specimen and no central steel pipe in the single-layer elastomeric pad in the GCP-S specimen.

2.2. Material properties

The compressive strength of the concrete cubes was tested in accordance with the *Standard for test method of mechanical properties on ordinary concrete* (GB/T50081-2002) [30]. The average 28-day compressive strength of concrete cubes was 32.28 MPa. The elastic modulus of concrete was 32.5 GPa. The average yield strength and tensile strength of the longitudinal reinforcement and the transverse stirrup were tested in accordance with the *Metallic materials–Tensile testing at ambient temperature* (GB/T228-2002) [31]. The test results are shown in Table 2. Note that HRB400 and HRB335 reinforcement bars are the most commonly used steel rebar grades in engineering structures of China. The compressive strength of the no-shrinkage grout for anchoring longitudinal reinforcement extended from the precast bridge column are provided by the supplier. The properties of the grout are presented in Table 3. Parameters of the corrugated metal duct pre-embedded in footings are presented in Table 4. The supplier provided the parameters of elastomeric material in the built-in laminated pad and single-layer pad. The rubber had shore hardness of 65 and shear modulus of 0.55 MPa. The bond strength between the rubber and steel was more than 10 MPa. The tensile strength of the rubber was more than 18 MPa. The design compressive stiffness of the laminated rubber pad and single rubber pad were 685.7 kN/mm and 612.8 kN/mm, respectively.

2.3. Testing setup and loading protocol

Quasi-static cyclic tests were performed on all specimens in the Key Laboratory of Urban Security and Disaster Engineering of Ministry of Education at Beijing University of Technology, China. Fig. 5 shows the sketch of elevation view and testing photo of the test setup. During the test, a constant axial load of 360 kN was applied by a jack at top of the loading block of RC columns. This load corresponds to an ALI of about 13.3%, which is within the commonly used ALI range of 0.1–0.2 in China. The horizontal load was applied through a hydraulic actuator with load capacity of 500 kN.

Fig. 6 shows the loading protocol. Two different loading modes were applied to the RC bridge column during the tests. Force control mode was first applied before concrete cracking occurred in the plastic hinge of the RC specimen, and then the displacement control mode was adopted. The lateral displacement control mode included four stages. First, the specimens were loaded to 2 mm. Second, the lateral displacement was increased from 5 mm to 20 mm with an interval of 5 mm. Third, the lateral displacement levels started from 20 mm to 40 mm with an interval of 10 mm. At last, the displacements were applied from 40 mm to 140 mm with an interval of 20 mm. Two repetitive cycles were performed at each level. The loading process was terminated when the lateral strength of the specimen dropped to 85% of its maximum strength.

Two linear variable displacement transducers (LVDTs) were installed at the sides of the center of loading block in the loading direction, one at each side. Two load cells were used to record the axial load

Table 2
Property parameters of longitudinal reinforcement and transverse stirrups.

Type	Grade	Diameter (mm)	Yield strength (MPa)	Tensile strength (MPa)	Fracture strain (%)
Long. Rein.	HRB400	16	533	741	17.9
Trans. stirrup	HRB335	8	455	630	19.9

Table 3
Properties of the Low-shrinkage grout.

Item	1-day strength (MPa)	3-day strength (MPa)	28-day strength (MPa)	Vertical expansion rate (%)
Testing value	35	62	92	1.0

applied by the jack and the lateral load in the horizontal actuator, respectively (see Fig. 5).

3. Experimental results

3.1. Apparent failure modes

Fig. 7 shows the damage failure patterns of tested specimens at the end of the cyclic testing. It could be seen that the bending failure mode of the GCP specimen was similar to that of the CIP specimen, and both showed typical flexural failure mode. When loading was applied to the column, transverse cracks firstly appeared along the loading direction and extended along the height of RC specimen. With the increase of the lateral cyclic loads, the transverse cracks became wider and slanted downward, resulting in the massive concrete spalling and exposure of the longitudinal reinforcement and stirrups in the plastic hinge zones, as shown in Fig. 7(a) and (b). The height of concrete spalling was about 200mm in the plastic hinge zone of the CIP and GCP specimens. Fig. 7(c) and (d) present the failure modes of GCP-M and GCP-S specimens, respectively. As seen in these two figures, for the GCP-M and GCP-S models, only some cracks were developed at the bottom of the specimens, while no concrete spalling was observed during the tests until the models were completely damaged. Bending deformation was mainly concentrated on the built-in elastomeric pad and the cover concrete of the column was not severely damaged. Based on these observations, it is evident that incorporating elastomeric pad into the plastic hinge zone of the bridge column can effectively control the damage of the column. It was also found that the laminated elastomeric pad was more effective than the single elastomeric pad in reducing the cover concrete damage. Fewer and generally shorter cracks were observed when laminated elastomeric pad was installed. The deformation behavior of laminated elastomeric pad and single-layer elastomeric pad was founded to be substantially different during the compression-bending loading of the bridge columns. The single layer elastomeric pad clearly dilated under compressive forces as shown in Fig. 7(d), while no such damage was observed in the laminated elastomeric pad in Fig. 7(c). This is because the shims in the laminated elastomeric pad restrained the dilation of rubber layer, which made the laminated elastomeric pad less vulnerable to the bulge damage.

3.2. Deformation of unbonded longitudinal steel bars

Although lateral loading was applied at the side center of the loading block, slight torsion of the loading block is inevitable because of accidental eccentricity during the construction and imperfect installation between the actuator and loading block. The torsion deformation of the loading block may have effect on seismic behavior of the column, especially for the column with a built-in elastomeric pad. Therefore, two LVDTs were installed at the two sides of the center of the loading block to measure the cyclic lateral displacement in the loading direction. In Fig. 8, N and S represent the north and south locations of these two LVDTs, respectively. Torsional behavior was found during the lateral loading tests of the GCP-M and GCP-S specimens. The torsional angle at the loading block can be calculated as follows:

$$\theta = \frac{\Delta_1 - \Delta_2}{L_0} \tag{3}$$

where Δ_1 and Δ_2 are the measured displacements by the two LVDTs at the two sides of the loading block, respectively. L_0 is the horizontal distance between these two LDVTs, which was 720 mm in these tests.

Fig. 9(a) and (b) show the relationship of the torsional angles with loading time at the top of the GCP-M and GCP-S specimens during the tests, respectively. It can be seen that the torsional angles at the top of the GCP-M specimen increased cyclically with the loading time (i.e. the lateral loading displacement), but the torsional angle at the top of the GCP-S specimen increased monotonically with the loading time. The torsional deformation was displayed in these two specimens with different elastomeric pad details. The maximum torsional angle was 0.01 rad for the GCP-M specimen, which was smaller than that for GCP-S specimen, 0.043 rad. This torsional angle is mainly from the built-in elastomeric pad. The reasons for this are discussed in the following.

The longitudinal rebars along the height of elastomeric pad were unbonded in the GCP-S and GCP-M specimens. They would undergo nonlinear tension-compression cyclic strain during the cyclic lateral loads. When the elongated unbonded rebars was compressed, lateral deformation of rebars would be restrained along the radial direction by central steel pipe and steel sheets in the elastomeric pad (GCP-M specimen) or other rebars (GCP-S specimen). Therefore, the lateral deformation of rebars would be formed along the tangent direction of a circle with a radius of distance from rebars to center of the column. Then, it would impose torsional deformation of elastomeric pad, which had flexible torsional stiffness. For the GCP-S specimen, shear deformation was monotonically increased with the loading displacement of the column, imposing monotonous torsional deformation on elastomeric pad, as shown in Fig. 9(b). However, for the GCP-M specimen, the unbonded rebars buckled at its center height location when they were compressed, imposing torsional deformation of elastomeric pad at the same height. Therefore, it would impose slight torsional action on the upper RC column, as shown in Fig. 9(a). In order to observe the lateral deformation of the unbonded longitudinal steel bars within the height of the elastomeric pad, the laminated and single-layer elastomeric pads were cut from the GCP-M and GCP-S specimens after the tests, as shown in Fig. 10 and Fig. 11, respectively. As seen in Fig. 10(b), obvious buckling and anticlockwise twisting are observed in the middle portion of the unbonded longitudinal steel bars except that the bar No.12 was fractured at a drift ratio of 9.4%. Shear deformation of the unbonded longitudinal steel rebars within the height of single-layer elastomeric pad was observed from Fig. 11(b), which was essentially different from that in Fig. 10(b). The length of unbonded part was significantly shorter in the GCP-S specimen. Two rebars No.12 and No. 1 fractured at a drift ratio of 3.5% and 5.1%, respectively, obviously earlier than that happened in GCP-M specimen.

The maximum lateral deformation of each unbonded steel rebar was measured from the deformed rebars in Figs. 10(b) and 11(b). They are

Table 4
Parameters of the corrugated metal ducts.

Material	Length (mm)	Inner diameter (mm)	Thickness (mm)	Ripple Height (mm)	Radial stiffness (N/mm)
Carbon steel	500	55	0.3	2.5	800

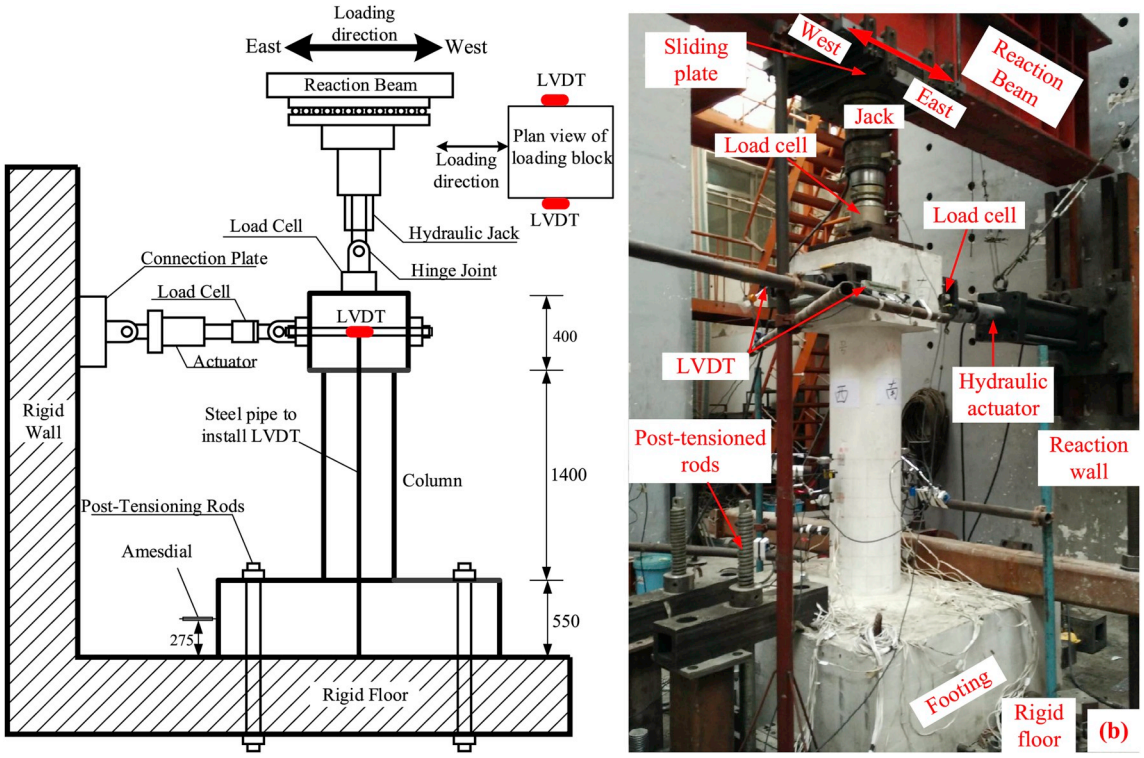

Fig. 5. Tests setup (unit: mm): (a) elevation view; (b) installation of the specimens.

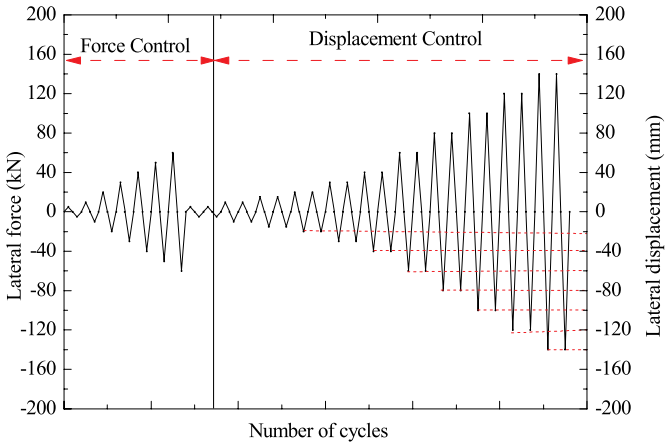

Fig. 6. Loading protocol of the cyclic tests.

listed in Table 5 for the GCP-M and GCP-S specimens. The average lateral deformation of the unbonded part of longitudinal rebars within the height of elastomeric pad was 18 mm and 5.2 mm for the GCP-M and GCP-S specimens, respectively. The maximum deformation angle of the unbonded longitudinal steel rebars could be estimated as:

$$\theta' = \frac{\Delta'}{r} \tag{4}$$

where Δ' is the maximum torsional deformation of unbonded steel rebars, r is the distance from the rebars to the center of elastomeric pad, which was 159 mm in this test. As seen in Fig. 10(b), it is found that the maximum torsional deformation was located at the center height of the unboned part of the longitudinal rebars, as a result of buckling behavior along the tangential direction. That is to say, the center height of the laminated elastomeric pad was twisted along the counterclockwise direction. The torsional angle at mid height of the laminated elastomeric pad could be calculated as $\theta' = \Delta'/r = 20/159 = 0.126$ rad according to the maximum lateral deformation of the unbonded longitudinal steel rebars. It was about 12.6 times of the torsional angle at the top of bridge column specimen, which was 0.01 rad as calculated above. It is seen in Fig. 11(b) that for the GCP-S specimen, the tangential deformation of the longitudinal steel rebars was the torsional deformation of the upper connection steel plate of the single-layer elastomeric pad. So the torsional angle of the upper connection plate of the single-elastomeric pad was $\theta' = \Delta'/r = 7.5/159 = 0.047$ rad, which was similar to the torsional angle at the top of the GCP-S specimen. That is: the torsional deformation of GCP-S specimen was mainly from the torsion of the single-layer elastomeric pad.

According to the above analysis, the test results showed that the torsional deformation at the top of the bridge column with single-layer elastomeric pad was almost the same as that of the single elastomeric pad. In addition, most torsional deformation of the specimen was concentrated at the rubber pad at the bottom of the specimen. This is mainly because the torsional stiffness of the bridge column is much higher than that of the elastomeric pad. Therefore, it is believed that the elastomeric pad with single-layer thick rubber will reduce the torsion stiffness of the column to a certain extent if no torsion restrained details are considered in the elastomeric pad. Furthermore, the test results also revealed that the torsional deformation of the GCP-S specimen (0.047rad) was much larger than that of the GCP-M specimen. This demonstrates the benefit of incorporating the laminated elastomeric pad into bridge columns. However, it is worth noting that the unbonded longitudinal steel bars buckled severely along the height of the laminated rubber element since no torsion restraint details was included in the laminated elastomeric pad and the height of laminated elastomeric pad was relatively large. A torsion restraint detail is recommended to prevent the twisting of the elastomeric pad caused by buckling of unbonded longitudinal rebars in the unbonded region, especially for the laminated elastomeric pad. Severe buckling of longitudinal rebars and torsional deformation of elastomeric pad are likely to reduce the lateral strength of bridge columns especially during large lateral displacement.

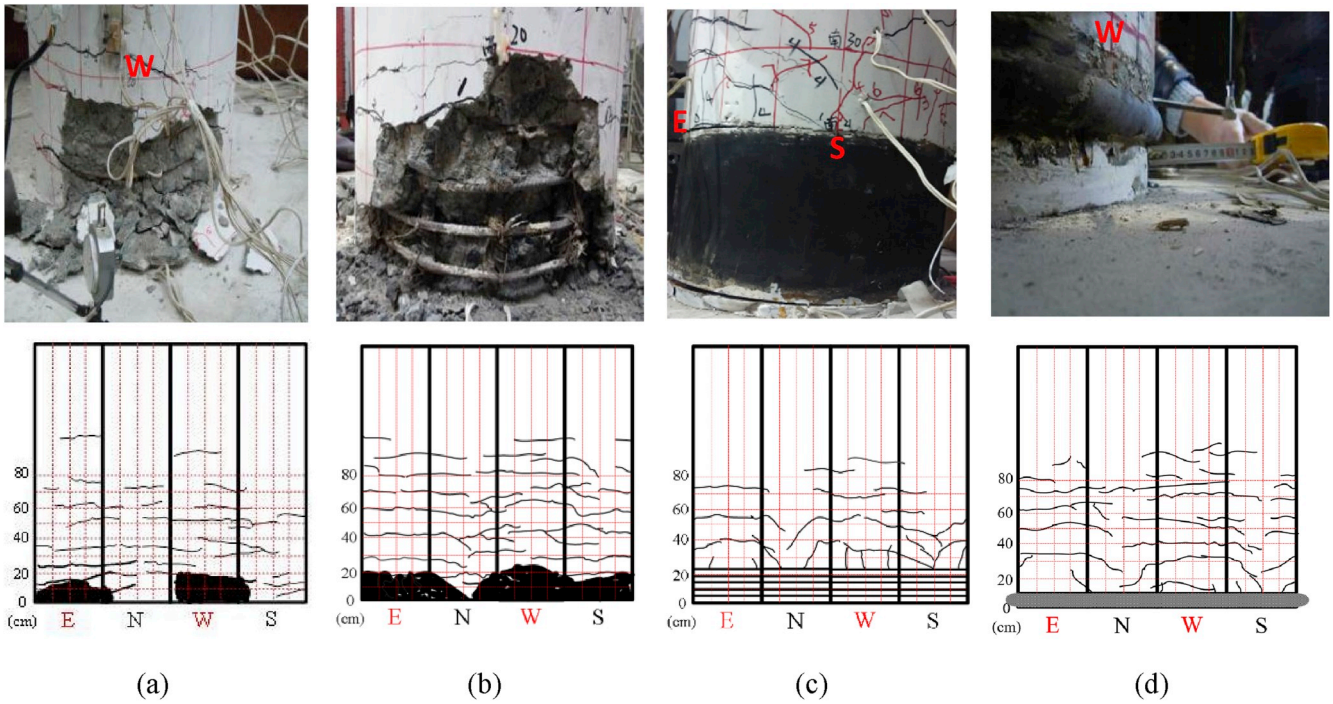

Fig. 7. Failure modes of the tested RC bridge column specimens: (a) CIP; (b) GCP; (c) GCP-M; (d) GCP-S.

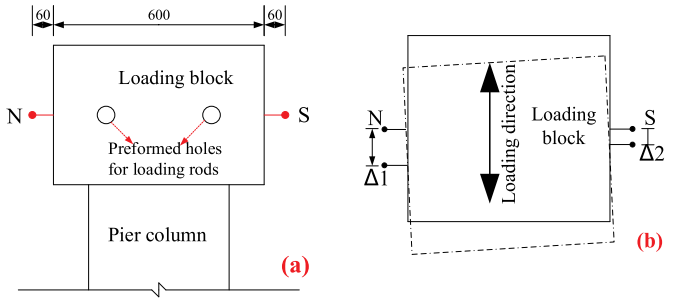

Fig. 8. Measurement of torsional displacement at the loading block of bridge column specimens, (a) elevation view, (b) top view.

3.3. Hysteretic curve

Fig. 12 shows the lateral force-displacement (drift) hysteretic curves of the tested specimens. Table 6 summarizes the key seismic performance parameters of these specimens. Note that the yield displacements were determined by the common graphing method [27], and the ultimate displacement is defined as the displacement corresponded to the lateral strength, which is 85% of the peak strength.

It is seen from Fig. 12(a) that the CIP specimen deformed almost linearly during the first eight cycles when the applied displacement was less than 15 mm. With the increase of the lateral displacement, the column exhibited obvious nonlinear behavior. The hysteretic curve of the CIP specimen was almost symmetric in the positive and negative loading directions, and the maximum lateral resistance strength in each loading cycle of the column decreased slightly. The hysteretic curve of the GCP specimen shown in Fig. 12(b) presented similar performance as the CIP specimen. Compared with the CIP and GCP specimens, the GCP-M and GCP-S specimens exhibited significantly different hysteretic behaviors. A prominent pinching effect was observed in the hysteretic curves of the CIP and GCP specimens shown in Fig. 12(a) and (b), but no such pinching effect was found in that of the GCP-M and GCP-S specimens. A bilinear hysteretic behavior is exhibited in Fig. 12(c) and

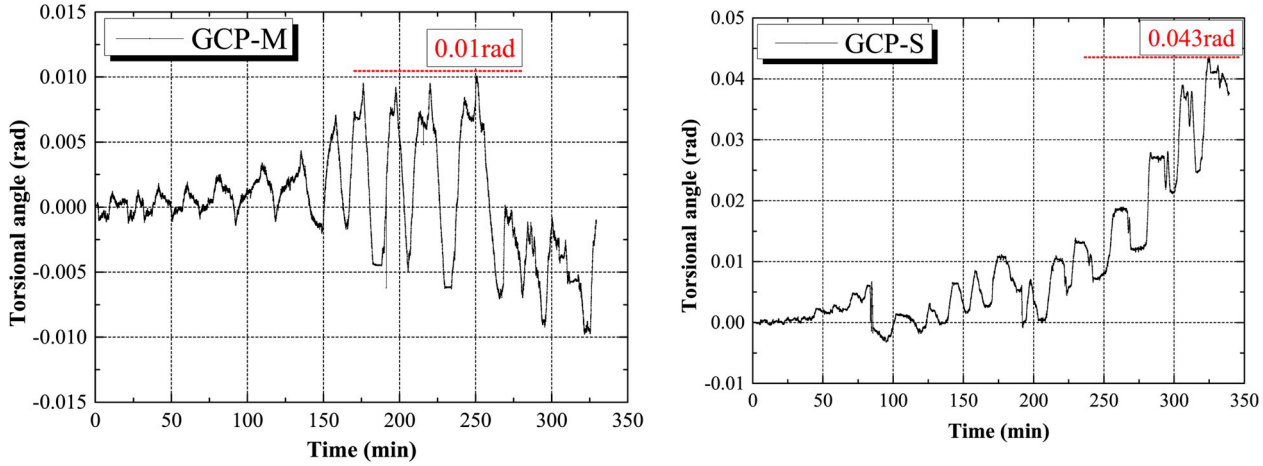

Fig. 9. Torsional angle at the loading blocks of tested specimens: (a) GCP-M specimen; (b) GCP-S specimen.

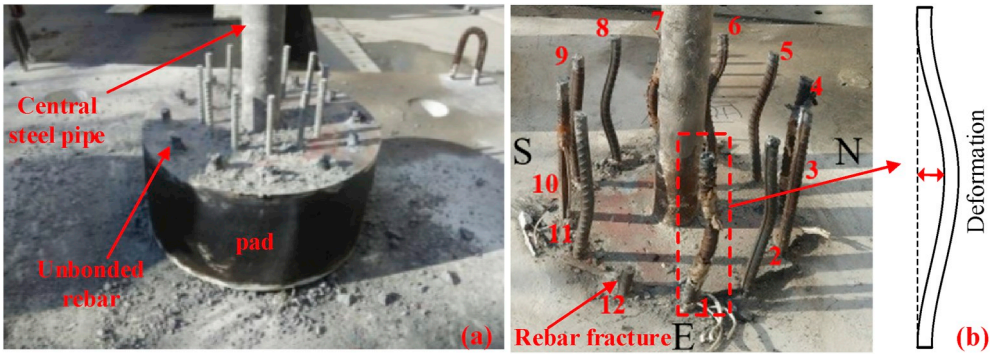

Fig. 10. Unbonded longitudinal steel bars in the GCP-M specimen: (a) laminated rubber pad cut from the column; (b) buckling modes of the rebars after the tests.

(d) until the unbonded longitudinal steel reinforcement within the height of elastomeric pad fractured. The main reason for this difference was that the sources of energy dissipation in these specimens were different. For the CIP and GCP specimens, the energy was mainly dissipated by the crushing of concrete in the plastic hinge region and yielding of the longitudinal rebars and transverse stirrups. However, the energy dissipation of the GCP-M and GCP-S specimens mainly came from the yielding of the unbonded longitudinal reinforcement at the bottom of the columns. It was also found that the longitudinal steel rebars in the GCP-M specimen fractured when the lateral loading displacement exceeded 140mm, which was much larger than that in the GCP-S specimen (i.e. 60mm). Because the unbonded length of longitudinal rebars in the GCP-S specimen was much smaller, resulting in stress concentration in the unbonded part.

Table 6 shows that compared to the CIP specimen, the GCP-based specimens (GCP, GCP-M and GCP-S) resulted in larger displacement capacity (yield and ultimate displacements), but smaller load resistance (the yield, ultimate and peak load). One exception is that the GCP-S specimen had slightly smaller ultimate displacement than that of the CIP specimen. The reason was that the length of unbonded rebars in single elasmomeric pad (GCP-S) was too small so that stress concentration was induced and premature rebar fracture would occur and result in smaller ultimate displacement. The larger displacement capacity in all GCP-based specimens was because the GCP-based specimens were connected to the precast footing by the grouted corrugated metal ducts, and the joint opening between the precast column and footing imposed larger displacement capacity. The post-grouted column-to-footing joint and the unbonded length of longitudinal rebars imposed substantial effect on the integrity of the GCP-based specimens. This effect was most evident in the GCP-M specimen (see Table 3), which had the largest yield and ultimate displacements but the smallest yield, ultimate and peak forces among these three GCP-based specimens.

3.4. Backbone curve

Fig. 13 shows the backbone curves of four tested specimens. The skeleton curves of the CIP and the GCP specimens were essentially similar in terms of almost all performance parameters, including loading stiffness, displacement and lateral resistance characteristics. The backbone curves of the GCP-M and GCP-S specimens were similar, but they were substantially different with those of the CIP and GCP specimens. Based on Table 6 and Fig. 13, the peak lateral and ultimate forces of the GCP-M and GCP-S specimens were slightly lower than those of the CIP and GCP specimens.

The lateral stiffness of a RC column can be described by the initial loading stiffness and equivalent stiffness. The initial stiffness refers to the tangent slope in the elastic stage of the force-displacement skeleton curve. In this study, the initial stiffness k_0 of the tested specimens was calculated based on the backbone curve shown in Fig. 13. The results are presented in Table 7. It is seen that the initial stiffness of the GCP specimen (9.94 kN/mm) was slightly lower than that of the CIP specimen (10.84 kN/mm). On the other hand, the laminated elastomeric pad significantly reduced the initial stiffness of the GCP-M specimen, which was only 57.7% of the value of the GCP specimen. It is interesting to find that when the single elastomeric pad was installed, the stiffness of the GCP-S specimen was similar with the values for the CIP and GCP specimens because the height of the elastomeric pad was small. The peak secant stiffness, which was the slope of the line connecting the peak strength point and the origin point of the force-displacement curve, was computed to show the stiffness features of the tested specimens. The results are summarized in Table 7. It can be seen that the GCP-M and GCP-S specimens also had the minimum peak secant stiffness because of the larger displacement at the peak strength point.

3.5. Energy dissipation and equivalent viscous damping ratio

Fig. 14 shows the cumulative hysteretic energy curves of the testing

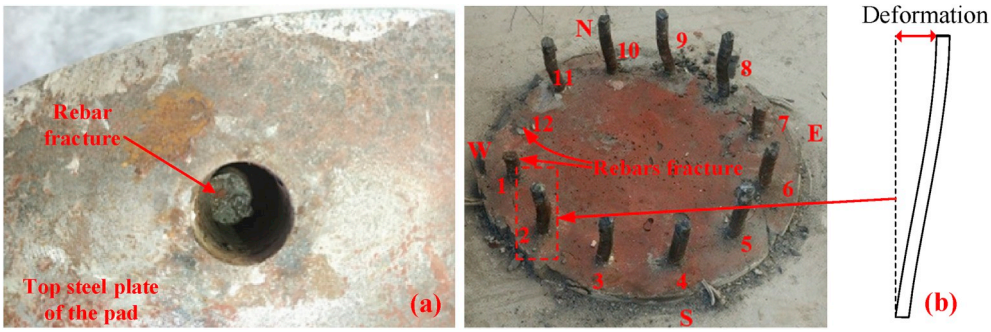

Fig. 11. Unbonded rebars in GCP-S specimen (a) Steel rebar fractured; (b) shear deformation of rebars.

Table 5
Deformations of the unbonded steel bars in different specimens (unit: mm).

Specimens	1	2	3	4	5	6	7	8	9	10	11	12
GCP-M	20	15.5	14.5	19.5	19	18.5	18	20	19.5	15	18	–
GCP-S	0	4.0	4.0	2.0	2.5	5.5	5.5	6.0	7.0	5.5	7.5	–

specimens. It is seen that when the laminated or single-layer elastomeric pad was incorporated into the GCP specimen, the energy dissipation capability of the column was increased even though less concrete damages occurred in the bottom of the specimen (see Fig. 7). It can be seen from Fig. 14 that the energy dissipation in specimen GCP-S was the highest among the four specimens up to the maximum displacement of 100 mm. However, the GCP-M and GCP specimens continued to dissipate energy for the displacement up to140 mm. As a result, the total dissipated energy exceeded that of the GCP-S specimen. The reason for the large amount dissipated energy in the GCP-S specimen until the displacement of 100 mm might be the stress concentration in the short unbonded length of longitudinal steel reinforcement in the plastic hinge region.

To further investigate the energy dissipation capability of the tested columns, the equivalent viscous damping ratio was computed by the following equation based on Priestley et al. [28]:

$$\xi_{eq,h} = \frac{1}{2\pi}\frac{A_1}{A_2} \tag{5}$$

where A_1 and A_2 are the shaded area as shown in Fig. 15, which represents the hysteretic energy dissipation and the elasticity energy, respectively.

Fig. 16 shows the equivalent viscous damping ratio of the testing specimens. It can be seen that for the CIP and GCP specimens, the equivalent damping ratios increased obviously when the drift ratio of the specimens was larger than 1%, indicating the serious damage at the bottom of the specimens. The equivalent damping ratio of the CIP

Table 6
Summary of responses quantities of different specimens.

Specimens	Yield Disp. $\Delta y/mm$	Ultimate Disp. $\Delta u/mm$	Yield foce F_y/kN	Ultimate force F_u/kN	Peak force F_{max}/kN
CIP	19.4	103.9	106.3	100	117.7
GCP	25.9	124.6	101.6	99.6	117.1
GCP-M	30.5	159.4	78.2	92.3	107.8
GCP-S	21.8	102.0	82.8	94.3	111.0

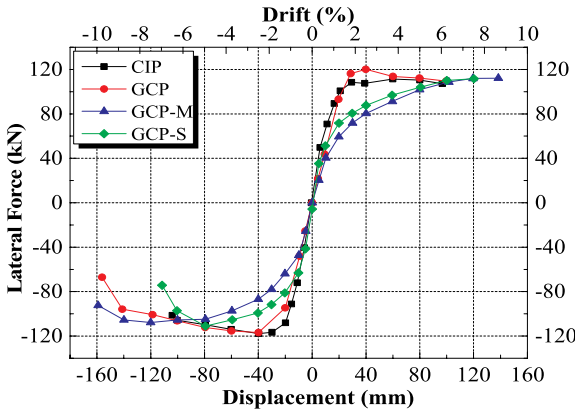

Fig. 13. Force-displacement skeleton curves for different specimens.

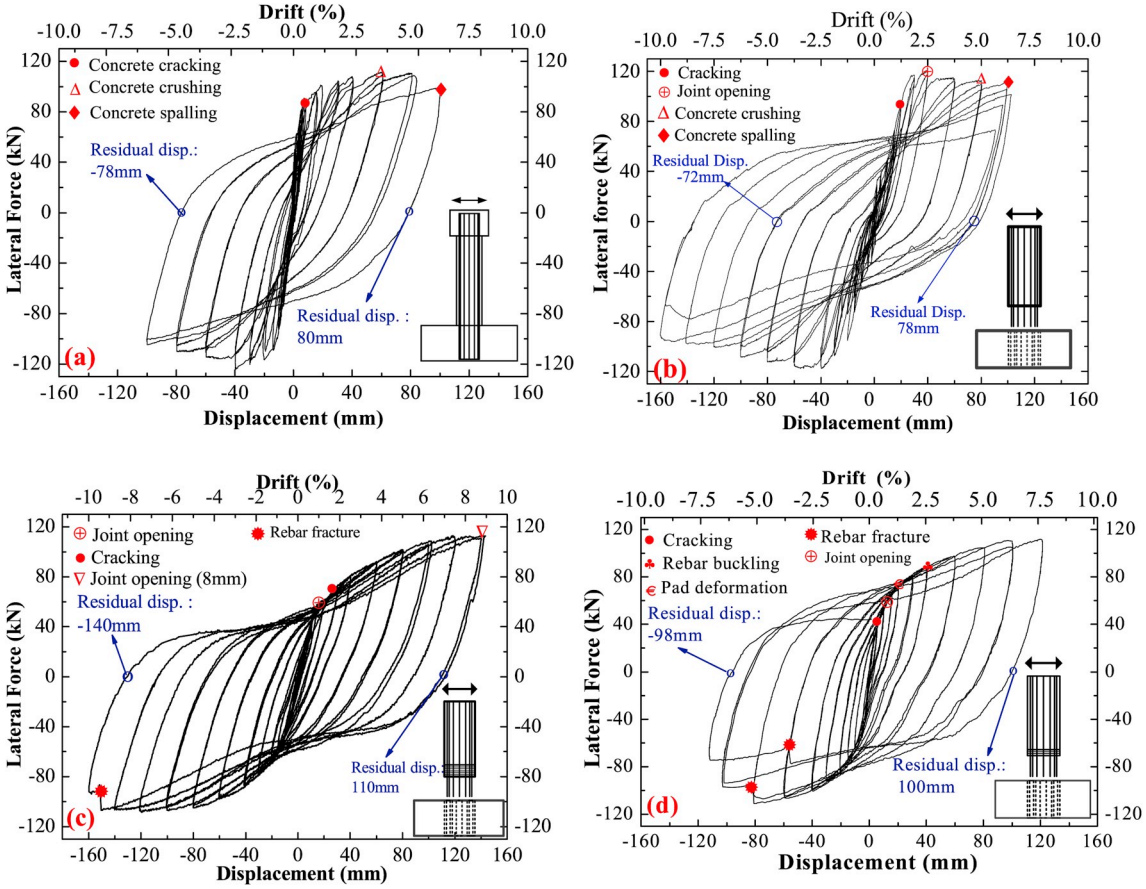

Fig. 12. Force-displacement hysteretic responses for tested specimens: (a) CIP; (b) GCP; (c) GCP-M; (d) GCP-S.

Table 7
Initial and peak equivalent stiffness of tested specimens.

Stiffness	CIP	GCP	GCP-M	GCP-S
Initial lateral stiffness k_0 (kN/mm)	10.84	10.44	5.75	10.67
Peak equivalent stiffness k_P (kN/mm)	3.81	2.98	0.81	1.39

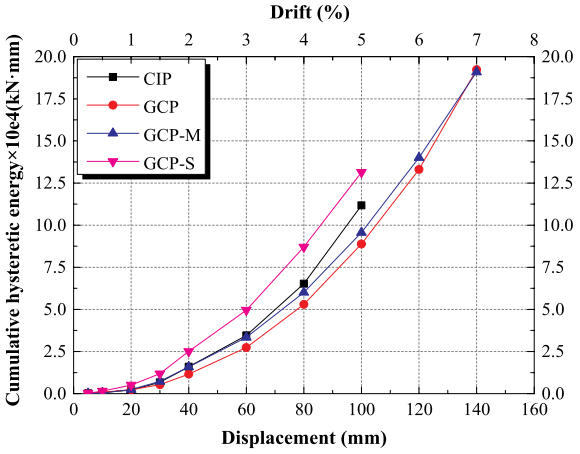

Fig. 14. Relationship between cumulative hysteretic energy and displacement.

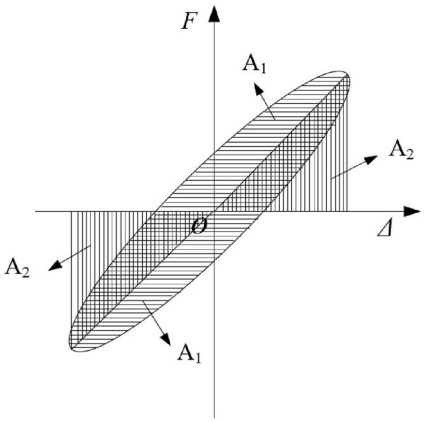

Fig. 15. Equivalent damping ratio calculation.

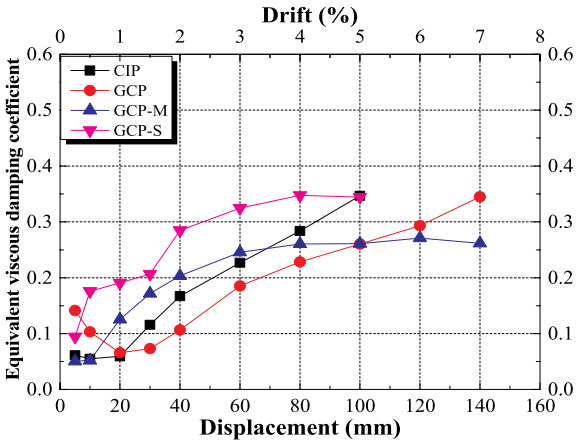

Fig. 16. Equivalent viscous damping coefficient of testing specimens.

specimen was larger than that of GCP specimen at the same drift ratio, indicating more severe damage in the CIP specimen. When the drift ratio was smaller than 1%, it is interesting to see that the equivalent damping ratio decreased slightly especially in the GCP specimen. The similar phenomenon was also reported by Guo et al. [32] and Wang et al. [33] when they examined the cyclic performance of reinforced concrete columns with chloride-induced corrosion in marine environment. They attributed this phenomenon to the experimental error. Since when the lateral displacement was small, the dissipated energy was very sensitive to the testing data. A small experimental error may significantly affect the calculated equivalent damping ratio [32].

For the GCP-M and GCP-S specimens, the equivalent damping ratio increased obviously when the drift ratio was smaller than about 3%. Beyond this point, the equivalent damping ratio was almost constant. This trend was different from that of the CIP and GCP specimens. This is because the energy dissipation of the GCP-M and GCP-S specimens was mainly from the yielding of the unbonded longitudinal rebars surrounded by the elastomeric pad. However, when the drift ratio reached certain level (about 3% in this study), no more damping source was added in these specimens except for unbonded longitudinal rebars, resulting in the constant damping ratio.

4. Discussion

4.1. Issues on durability of elastomeric pads

An elastomeric pad was incorporated into the precast RC bridge column with grouted corrugated metal ducts in this study. The durability of elastomeric pad will be a main concern for this novel design concept. The aging effect is the key problem of elastomeric pad. The specific detail of the elastomeric pad used in this study was similar to that of laminated rubber bearing which have been already studied and applied in many buildings and bridges all over the world. The mechanical performance of elastomeric bearing will degrade to some extent but it is not so critical in the service of 50 years even 100 years according to the engineering practice and many research results. The vertical stiffness increased by +7% and the post-yield stiffness increased by +6% for a lead rubber bearing were observed by accelerated aging tests to simulate the service time of 60 years [34]. Some seismic analyses were carried out for isolated RC bridges by considering stiffness change caused by aged rubber bearings for 50 years and 100 years [35,36]. It was found that the moment and shear forces of an isolated bridge where aging has occurred for 100 years decreased by 0.8% and 1.2%, respectively. Thermal aging of the laminated rubber bearing had no significant effect on the structural system of the whole bridge. The rotational performance of the built-in elastomeric pad was used in this study, and the thermal aging was considered to have slightly adverse effect on the lateral stiffness of the precast bridge columns. All of these researches provide support that the aging effect on durability of precast columns with elastomeric pad will not be critical.

4.2. Design consideration for the height of elastomeric pads

A reduced initial lateral stiffness of the precast bridge column specimen with built-in elastomeric pad was observed in this study. The initial stiffness of the GCP-M specimen was 5.75 kN/m, which reduced by 45% compared to the GCP specimen. It is noted that the lateral stiffness was dependent on the design details of the elastomeric pad, especially on the height of laminated pad. The height of elastomeric pad was 200 mm in the GCP-M specimen, and 65 mm in the specimen GCP-S. The initial lateral stiffness of the former one was notably less than that of the latter. The reduced lateral stiffness of precast columns will impose adverse effects on seismic responses of the whole bridge system. The test results revealed that there was no critical reduction of lateral stiffness for the novel bridge columns if the height of the elastomeric pad was small, such as the specimen GCP-S. The main problem was how to balance the height of the elastomeric pad and the reduction of lateral stiffness. An appropriated height of the laminated elastomeric pad should be determined to ensure sufficient lateral stiffness and energy

dissipation capacity and to eliminate the concrete damage at the bottom of precast bridge columns, simultaneously.

4.3. Recommendations for torsion-resistance details

In this experiment, a torsional deformation of the elastomeric pad was observed in the precast bridge columns with a flexible elastomeric pad in the plastic hinge region. The torsional angle was 0.126 rad and 0.047 rad for the GCP-M and GCP-S specimens, respectively. In engineering practice, if the superstructure restrains the torsional deformation of columns in rigid bridges, then the torsional movement of single-layer elastomeric pad will be restrained by the column. However, it is hard to avoid the buckling behavior of unbonded longitudinal rebars on account of insufficient torsion-resistance stiffness of laminated elastomeric pad with large height as shown in Fig. 10. Buckling of rebars colud result in adverse effect on energy dissipation. A rectangular or square central steel tube is recommended to be inserted into the built-in laminated elastomeric pad in the precast bridge column to prevent the excessive torsional deformation. Then the drilled holes within elastomeric pad can provide sufficient buckling restraint for unbonded longitudinal rebars of the bridge column.

5. Conclusions

An elastomeric pad detail was incorporated into precast RC bridge columns with grouted corrugated metal duct connections. The objective was to improve the energy dissipation capacity and to alleviate concrete damage at the bottom of the precast bridge columns. Four 1/4-scaled bridge column specimens were designed and tested under constant axial loads and cyclic lateral loads to investigate the seismic performance of precast bridge columns with/without elastomeric pad in plastic hinge region. They are: cast-in-place RC bridge column (CIP) as a benchmark specimen, a precast RC column with grouted metal corrugated duct connection (GCP), a GCP column with a built-in laminated elastomeric pad (GCP-M), and a GCP column with a built-in single layer elastomeric pad (GCP-S). The following conclusions are drawn based on this study.

(1) The four specimens evaluated by quasi-static tests exhibited acceptable but different seismic performance. The precast RC columns had comparative or even more preferable seismic performance, and significant advantages of accelerated bridge construction than the CIP specimen. The GCP-S specimen showed better energy dissipation and minor concrete damage of the column bottom than the GCP specimen. The GCP-M specimen could present most promising and suitable seismic performance for precast bridges if an optimal height of the laminated elastomeric pad is determined.
(2) The GCP specimen had comparable seismic performance to that of the CIP specimen with respect to the failure mode, lateral strength, displacement ductility, energy dissipation and residual displacement. There was no bond-slip failure between grouted metal corrugated duct and its inner anchored longitudinal steel reinforcement. It is concluded that grouted corrugated duct connection is reliable for application in high seismic zones.
(3) For the GCP-M and GCP-S specimens, no apparent damage of the elastomeric pad was observed even after the precast bridge column lost its lateral loading capacity. The reduced concrete damage at the bottom of precast columns and the obvious torsional deformation in the elastomeric pad were observed because of the weak torsional stiffness of the elastomeric pad.
(4) The GCP-M and GCP-S specimens have reduced initial stiffness and improved energy dissipation capacity, but without severe concrete damage in the column. The longitudinal steel reinforcement in the drilled holes within the elastomeric pad were prematurely fractured if the unbonded length was not enough.
(5) It is recommended that the built-in laminated elastomeric pad (e.g. GCP-M) is more suitable to be used in precast bridge columns than thin, single layer elastomeric pads (e.g. GCP-S). An optimized height of the built-in laminated elastomeric pad should be determined to obtain a balance between the initial stiffness and energy dissipation of the precast bridge column.

Acknowledgements

This research was financially supported by the National Natural Science Foundation of China under Grant No. 51578030 and 51778024, Beijing Nova Program under Grant No. Z181100006218053, the Importation and Development of High-Caliber Talents Project of Beijing Municipal Institutions under Grant No. CIT&TCD201704027. Their supports are gratefully acknowledged.

References

[1] Shahawy M. Prefabricated Bridge Elements and Systems to limit traffic disruption during construction. Washington, D.C., USA: Transportation Research Board; 2003.
[2] Kapur J, Yen WP, Dekelbab W, Bardow A, Keever M, Sletten J, et al. Best practices regarding performance of ABC connections in bridges subjected to multihazard and extreme events. 2012. No. NCHRP Project 20-68A.
[3] Mashal Mustafa, Palermo Alessandro. Emulative seismic resistant technology for accelerated bridge construction. Soil Dyn Earthq Eng 2019https://doi.org/10.1016/j.soildyn.2018.12.016.
[4] Tazarv M, Saiid Saiidi M. Low-damage precast columns for accelerated bridge construction in high seismic zones. J Bridge Eng 2015;21(3):04015056.
[5] Mislinski SJ. Anchorage of grouted connectors for a precast bent cap system in seismic regions. Sacramento: California State University; 2003.
[6] Pang JBK, Eberhard MO, Stanton JF. Large-bar connection for precast bridge bents in seismic regions. J Bridge Eng 2009;15(3):231–9.
[7] Alireza Mohebbi, Saiid Saiidi M, Ahmad Itani. Development and seismic evaluation of pier systems w/pcket connections, CFRP tendons, and ECC/UHPC columns Reno: University of Nevada; 2017. Report No. CCEER 17-02.
[8] Sprinkel M. Prefabricated bridge elements and systems. NCHRP Synthesis of Highway Practice; 2008.
[9] AASHTO. AASHTO guide specifications for LRFD seismic bridge design. AASHTO; 2009.
[10] Marsh ML. Application of accelerated bridge construction connections in moderate-to-high seismic regions. Transp Res Board; 2011.
[11] Restrepo J, Matsumoto E, Tobolski M. Development of precast bent cap systems for seismic regions. NCHRP Report 2011;681.
[12] Steuck KP, Eberhard MO, Stanton JF. Anchorage of large-diameter reinforcing bars in ducts. ACI Struct J 2009;106(4):506–13.
[13] Matsumoto E, Waggoner M, Sumen G, Kreger M, Wood S, Breen J. Development of a precast bent cap system. Center for transportation research, report No. 1748-02. Austin: University of Texas; 2001.
[14] Brenes FJ, Wood SL, Kreger ME. Anchorage requirements for grouted vertical-duct connectors in precast bent cap systems: a summary Austin, TX: Center for Transportation Research; 2006. Project Summary Report 0-4176.
[15] Chen J, Xiao Y, Yin Q. Bonding strength of rebar anchorage in embedded corrugated sleeve with high strength grout. J Build Struct 2015;36(7):140–7. [in Chinese)].
[16] Matsumoto E. Emulative precast bent cap connections for seismic regions: component test report—preliminary grouted duct specimen (unit 5). Report No. ECS-CSUS-2009-02. Sacramento: California State University; 2010.
[17] Belleri A, Riva P. Seismic performance and retrofit of precast concrete grouted sleeve connections. PCI J 2012;57:97–109.
[18] Popa V, Papurcu A, Cotofana D, Pascu R. Experimental testing on emulative connections for precast columns using grouted corrugated steel sleeves. Bull Earthq Eng 2015;13(8):2429–47.
[19] Tazarv M, Saiidi MS. Design and construction of UHPC-filled duct connections for precast bridge columns in high seismic zones. Struct Infrastruct Eng 2017;13(6):743–53.
[20] Mander JB, Cheng CT. Seismic resistance of bridge piers based on damage avoidance design 1997. Technical Report, NCEER 97-0014.
[21] Hieber DG, Wacker JM, Eberhard MO, Stanton JF. Precast concrete pier systems for rapid construction of bridges in seismic regions. Washington state transportation center (TRAC), report No. WA-RD 611.1. University of Washington and Washington State Department of Transportation; 2005.
[22] Kawashima K, Nagai M. Development of a reinforced concrete pier with a rubber layer in the plastic hinge region, Structural and Earthquake Engineering. Proc Jpn Soc Civ Eng 2002:113–28. 703/I-59.
[23] Motaref S, Saiidi M, Sanders D. Experimental study of precast bridge columns with built-in elastomer. Transp Res Rec: Transp Res Board 2010;2202(1):109–16.
[24] Cruz-Noguez CA, Saiidi M Saiid. Experimental and analytical seismic studies of a four-span bridge system with innovative materials. Reno, NV: Center for Civil Engineering Earthquake Research, Department of Civil Engineering, University of Nevada; 2010. p. 89557.
[25] Sarira Motaref, Saiid Saiidi M, Sanders David. Shake table studies of energy-dissipating segmental bridge columns. J Bridge Eng 2014;19(2):186–99.
[26] Varela Sebastian, Saiid Saiidi M. A bridge column with superelastic NiTi SMA and replaceable rubber hinge for earthquake damage mitigation. Smart Mater Struct

2016;25(7):075012.
[27] Dabiri H, Kheyroddin A. An analytical study into the seismic behavior of RC pier with elastomeric materials. Asian J Civ Eng 2017;18(7):1183–93.
[28] Ministry of transport of the people's Republic of China, specifications for design of highway reinforced concrete and prestressed concrete bridges and Culverts, JTG 3362-2018. 2018. [in Chinese)].
[29] Ministry of transport of the people's Republic of China, Guidelines for seismic design of highway bridges, JTG/T B02-01-2008. 2008. [in Chinese)].
[30] Standard for test method of mechanical properties on ordinary concrete, GB/T50081-2002. [in Chinese)].
[31] Metallic materials–Tensile testing at ambient temperature, GB/T228-2002. [in Chinese)].
[32] Guo A, Li H, Ba X, Guan X, Li H. Experimental investigation on the cyclic performance of reinforced concrete piers with chloride-induced corrosion in marine environment. Eng Struct 2015;105:1–11.
[33] Wang J, Wang Z, Tang Y, Liu T, Zhang J. Cyclic loading test of self-centering precast segmental unbonded posttensioned UHPFRC bridge columns. Bull Earthq Eng 2018;16(11):5227–55.
[34] Feng Demin, Takafumi Miyama, Masuda Keiji, et al. A detailed experimental study on Chinese lead rubber bearing. Proceedings of the 12th world conference of earthquake engineering, Auckland, New Zealand, january 30-februray 4. 2000. Paper No.0202.
[35] Kitahara T. Seismic performance of RC bridge piers considering aging of base isolated rubber. Proceeding of 4th international ASRANet conference. 2008.
[36] Ju Oh, Ho Kim Jin, Cho Yi Hwa. Effects of thermal aging of laminated rubber bearing on seismic performance of bridges. J Vibroeng 2016;18(6). 3782-2797.